RESEARCH ARTICLE

Check for updates

Liquid-phase epitaxial growth of multiple MOF thin films with high lattice mismatch†

Li-Mei Chang,[a,b] Zhi-Zhou Ma,[a,b] Jiandong Huang [ID][a] and Zhi-Gang Gu [ID] *[b,c,d]

The development of multiple metal–organic framework (MOF) thin films with high lattice mismatch is still a challenging task. Herein we report a series of single and multiple (bi-varietal and tri-varietal) pillar-layered MOF thin films (surface-coordinated MOF thin films, SURMOFs) $[Cu_2L_2dabco]_n$ (L = bdc, bpc and tpdc) with preferred [001]-orientation on the substrate surfaces using a liquid-phase epitaxial (LPE) layer by layer pump method. The single SURMOFs with the same c-lattice parameters but different a- and b-lattice parameters result in the successful growth of oriented multiple SURMOFs with high lattice mismatch (up to 77.8%). The vapor adsorption results show that the representative bi-varietal SURMOF with large lattice mismatch has different adsorption behavior from single SURMOFs, providing a new strategy to achieve tuning of the adsorption kinetics performance in sensing applications.

Metal–organic frameworks are constructed from metal nodes and organic linkers, which are a kind of crystalline porous material and are attracting great interest due to their diverse topological structures and attractive functionalities.[1–3] To date, MOFs have been promising candidates for guest adsorption and separation,[4–6] catalysis,[7–9] energy,[10–12] optoelectronic sensors and devices,[13–15] and biological applications.[16,17] Compared to single MOFs, multiple MOFs assembled from the conjugation of two or more MOF units have been emerging as hybrid materials for extending their functionalities and applications.[18–24] The different lattice parameters and strong chemical bondings between the heterostructured interface lead to the difficult growth of such multiple MOFs. Such heterostructured materials with high lattice mismatch will greatly expand the types of material candidates and improve their functionalities. Therefore, rational design of new multiple MOFs with high lattice mismatch is of great importance for their fundamental research and practical applications in various fields.

In the last decade, MOF thin films have been greatly prepared due to their large surface active sites, conveniently accessible in sensing and device applications.[25–32] Among the preparation methods of MOF thin films, the liquid-phase epitaxial (LPE) layer by layer method is realized for use in growth of MOF thin films (also called surface-coordinated MOF thin films, SURMOFs) on functionalized substrates, displaying unique features including high degree of controlled growth orientation, tunable thickness, and good homogeneity.[23,33–36] Recently, although some multiple MOF thin films have been reported,[34] obtaining multiple MOF thin films with high lattice mismatch is still a challenging task.

For preparing multiple MOF thin films with high lattice mismatch, in this work, a liquid phase epitaxy (LPE) layer by layer pump procedure (Scheme S1†) was used to yield oriented MOF thin films (referred to as SURMOFs). A series of multiple 3D MOF thin films are constructed from three isoreticular pillar-layered MOFs $[Cu_2L_2dabco]_n$,[38,39] $[Cu_2bdc_2dabco]_n$ (**SURMOF-a**) (bdc = 1,4-benzenedicarboxylate and dabco = diazabicyclo[2,2,2]octane), $[Cu_2bpdc_2dabco]_n$ (**SURMOF-b**) (bpdc = biphenyl-4,4′-dicarboxylate), and $[Cu_2tpdc_2dabco]_n$ (**SURMOF-c**) (tpdc = terphenyl-4,4-dicarboxylate). These MOFs are constructed from classic Cu^{2+} "paddle-wheel" units connected with three linear dicarboxylic acid ligands (H_2bdc, H_2bpdc, and H_2tpdc) to form layers along the [001] plane pillared by bitopic N-containing linkers as shown in Scheme 1. **SURMOF-a** and **SURMOF-b** have the same c-lattice parameters but 38.6% lattice mismatch in a- and b-lattice parameters while **SURMOF-a** and **SURMOF-c** have 77.8% lattice mismatch. They were selected to prepare the heterostructural SURMOFs on 11-mercapto-1-undecanol (MUD) SAM modified Au surfaces.[40] Using a home-made LPE layer by layer pump instrument,[41,42] mono-varietal SURMOFs (**SURMOF-a**, **SURMOF-b**, and **SURMOF-c**), bi-varietal SURMOFs (**SURMOF-b on a, SURMOF-c on a, SURMOF-a on b, SURMOF-c on b, SURMOF-a on c,** and
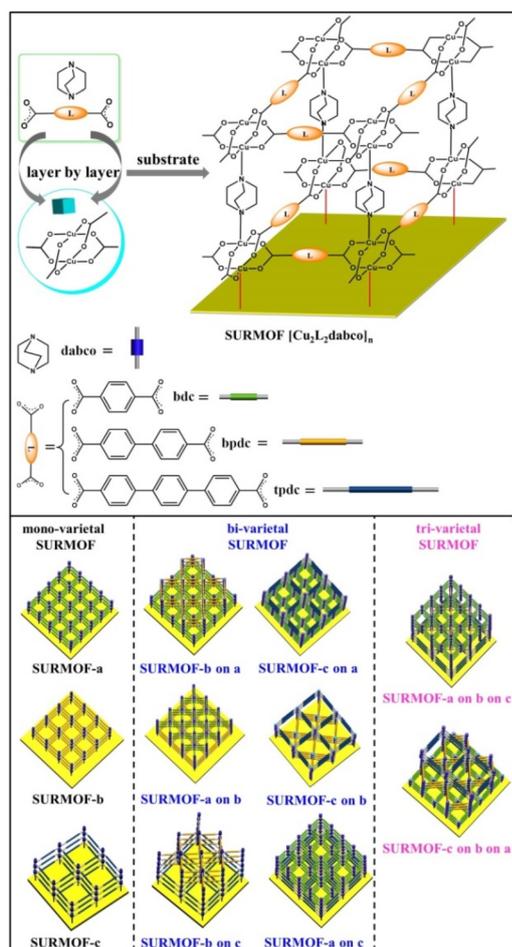
[a]*College of Chemistry, Fuzhou University, Fuzhou, Fujian 350108, China*
[b]*State Key Laboratory of Structural Chemistry, Fujian Institute of Research on the Structure of Matter, Chinese Academy of Sciences, Fuzhou, Fujian 350002, China. E-mail: zggu@fjirsm.ac.cn*
[c]*Institute of Functional Interfaces (IFG), Karlsruhe Institute of Technology (KIT), 76344 Eggenstein-Leopoldshafen, Germany*
[d]*Fujian Science & Technology Innovation Laboratory for Optoelectronic Information of China, Fuzhou, Fujian 350108, China*
†Electronic supplementary information (ESI) available. See DOI: https://doi.org/10.1039/d2qi02464k

1136 | *Inorg. Chem. Front.*, 2023, **10**, 1136–1142

This journal is © the Partner Organisations 2023

Scheme 1 Schematic illustration for the preparation of mono-varietal SURMOFs $[Cu_2L_2dabco]_n$ (L = bdc, bpdc, and tpdc) and their multiple (bi-varietal and tri-varietal) SURMOFs on substrate surfaces by using a LPE layer by layer method.

SURMOF-b on c), and tri-varietal SURMOFs (**SURMOF-a on b on c**, and **SURMOF-c on b on a**) with preferred [001]-orientation can be successfully prepared on the substrate surfaces. Since the length of a-lattice parameter ($a2$) in **SURMOF-b** is close to that of $\sqrt{2}a1$ (a-lattice parameter in **SURMOF-a**), the $a3$ (a-lattice parameter in **SURMOF-c**) is close to that of $\sqrt{2}a2$, and they have similar c-lattice parameters, and the MOF-on-MOF showed diagonal growth (see Scheme 1, bottom), leading to large lattice mismatch (38.6% and 77.8%). The quartz crystal microbalance (QCM) uptakes of ethoxyethane and mesitylene show that the multiple SURMOF has different adsorption behavior from single SURMOFs, demonstrating that the synergistic effect of the multiple SURMOF with large lattice mismatch has the advantage of tuning the adsorption kinetics performance, which provides new platforms to combine multiple functional MOF thin films for extending their sensing applications.

Pillar-layered SURMOFs $[Cu_2L_2dabco]_n$ (L = bdc, bpc and tpdc) consist of dicarboxylic acids, H_2bdc, H_2bpdc and H_2tpdc as layers and dabco as the pillar. The pore size of 3D

SURMOFs $[Cu_2L_2dabco]_n$ grown on substrate surfaces can be tuned by choosing appropriate dicarboxylate ligands. It's noted that a well-known binuclear "paddle-wheel" copper carboxylate complex $[Cu_2(COO)_4N_2]$ is in this series of SURMOFs, resulting in the formation of a 2D $[Cu_2L_2]_n$ layer.[37] The linear N-donor ligand dabco is coordinated to the Cu empty axial centers, forming a pillar that is perpendicular to $[Cu_2L_2]_n$ layers (Fig. 1a, b and c). The 3D pillar-layered isostructural SURMOFs possessed different lattice cells with the same c-lattice parameter. The lattice cell parameters are $10.8 \times 10.8 \times 9.5$ Å^3 for $[Cu_2bdc_2dabco]_n$, $14.9 \times 14.9 \times 9.5$ Å^3 for $[Cu_2bpdc_2dabco]_n$, and $19.2 \times 19.2 \times 9.5$ Å^3 for $[Cu_2tpdc_2dabco]_n$. The growth orientation of isostructural SURMOFs is along [001], which is shown in the XRD data in Fig. 1d, e and f.

It has been demonstrated that self-assembled monolayers (SAMs) containing functional groups are specially used as nucleation sites for epitaxial growth of MOF thin films.[43,44] The pillar-layered SURMOFs $[Cu_2L_2dabco]_n$ can be easily grown on the SAM surfaces by using the LPE layer by layer approach.[45–48] Since the preparation procedures of isoreticular SURMOFs (Fig. 2a, b and c) are similar, the preparation of **SURMOF-a** is described in detail. The OH-group functionalized Au substrate (Fig. S1†) was subsequently filled with $Cu(OAc)_2$ and H_2L/dabco (L = bdc, bpc and tpdc) ethanolic solutions in the sample cell of the pump system for 30 min at 50 °C. There was 2 min ethanol washing in each step. Then 30 repeated cycles of preparation process resulted in the formation of homogeneous **SURMOF-a, -b, -c**. Out-of-plane XRD patterns (Fig. 1d) showed two clear diffraction peaks located at 9.26° and 18.52°, corresponding to the (001) and (002) diffraction peaks in the XRD patterns simulated. The in-plane XRD patterns showed distinct peaks at 8.18°, 11.58°, 16.36°, and 18.34°, which are related to the (100), (1–10), (200), and (210) peaks. The high-quality out-of-plane and in-plane XRD patterns as well as the small width of the diffraction peaks clearly revealed the successful growth of highly crystalline **SURMOF-a** with its [001]-direction perpendicular to the substrate surface. Similarly, two clear peaks are located at the (001) and (002) diffraction peaks in the out-of-plane XRD patterns of **SURMOF-b** and **SURMOF-c**, respectively. The in-plane XRD peaks at 5.92°, 11.84°, 15.16°, and 17.78° are related to the (100), (001), (020), and (210) peaks (Fig. 1e) of **SURMOF-b**, while the distinct peaks at 4.62°, 9.24°, 13.78°, and 18.48° are related to the (100), (200), (300), and (400) peaks (Fig. 1f) of **SURMOF-c**, which clearly revealed the successful growth of highly crystalline **SURMOF-b** and **SURMOF-c** with their [001]-orientation. The IR spectra (Fig. S2†) of **SURMOF-a** exhibited two characteristic bands centred at 1628 cm^{-1}, which can be assigned to the COO vibrations of the carboxylate groups of the bdc linker, and provide additional evidence of the successful growth of **SURMOF-a**. Similarly, the IR spectra (Fig. S3 and 4†) of **SURMOF-b** (1624 and 1420 cm^{-1}) and **SURMOF-c** (1590 and 1425 cm^{-1}) revealed the symmetric and asymmetric –COO vibrations of the carboxylate groups from bpdc and tpdc linkers, and provide additional evidence of the successful
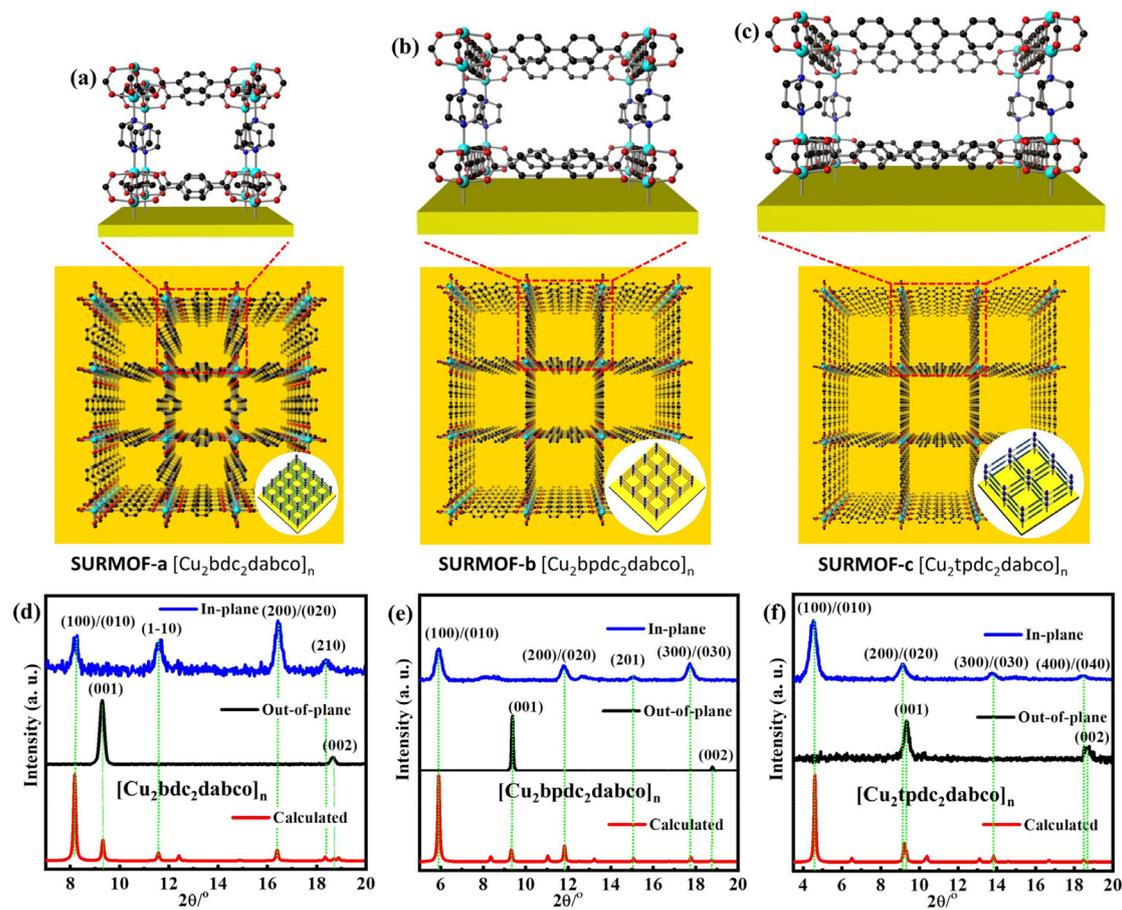
Fig. 1 The structure of mono-varietal SURMOFs: (a) **SURMOF-a**; (b) **SURMOF-b**; (c) **SURMOF-c**; the out-of-plane and in-plane XRD pattern of SURMOFs: (d) **SURMOF-a**; (e) **SURMOF-b**; (f) **SURMOF-c**.

growth of **SURMOF-b** and **SURMOF-c**. In addition, the surface SEM images (Fig. 2d and e) of the single (mono-varietal) SURMOFs prepared with 30 cycles clearly revealed homogeneous thin films.

For further preparation of heterostructural (bi-varietal and tri-varietal) MOF thin films, the LPE layer by layer pump method was still used to prepare multiple SURMOFs. Briefly, the pre-prepared **SURMOF-a** was used as the growth substrate, and then this layer by layer pump process allows us to separately control the Cu(OAc)$_2$ and organic linker H$_2$tpdc deposition on the **SURMOF-a** to form **SURMOF-c on a** (Fig. 2a). The out-of-plane XRD patterns (Fig. S6b†) of **SURMOF-c on a** showed a strong diffraction peak at 9.36° and weak peak at 18.80° corresponding to (001) and (002) diffraction peaks in the simulated XRD patterns (Fig. 2c). In addition, the related in-plane XRD patterns (Fig. 2c) contained both in-plane XRD peaks of **SURMOF-a** and **SURMOF-c**. These XRD patterns clearly displayed the successful growth of **SURMOF-c on a** with high crystallization along [001]-orientation on the functionalized substrate surface. The other bi-varietal SURMOFs (**SURMOF-a on b**, **SURMOF-a on b**, **SURMOF-c on a**, **SURMOF-a on c**, and **SURMOF-b on c**) can be prepared successfully using the same process, which can be demonstrated by the

XRD, SEM and IR data (see Fig. S6–11†). Furthermore, the tri-varietal SURMOF (**SURMOF-c on b on a**) was also prepared by using the LPE layer by layer pump method (Fig. 3a). The pre-prepared **SURMOF-a** was used as the growth substrate, and then the Cu(OAc)$_2$ and organic linker H$_2$bpdc were separately deposited on the **SURMOF-a** (30 cycles) to form **SURMOF-b on a**. Finally, Cu(OAc)$_2$ and organic linker H$_2$tpdc were separately deposited on the top of **SURMOF-b on a** to further form **SURMOF-c on b on a**. The successful growth was demonstrated by out-of-plane XRD patterns (Fig. 3b and c). The XRD pattern data clearly revealed that **SURMOF-c on b on a** possessed high [001] growth orientation. Meanwhile, the tri-varietal SURMOF **SURMOF-a on b on c** was successfully prepared using the same strategy as shown in Fig. S12 and 13.† The related IR spectra (Fig. S14†) of tri-varietal SURMOFs revealed their symmetric and asymmetric –COO vibrations from the carboxylate groups of the organic linkers.

To better understand the mismatched lattice of the heterostructural SURMOFs, we calculated the lattice mismatch by using the unit cell parameters of the mono-varietal SURMOFs. The $a1$, $a2$ and $a3$ are the lattice distances of **SURMOF-a**, **SURMOF-b** and **SURMOF-c**, respectively. Interestingly, the length of $a2$ is close to that of $\sqrt{2}a1$, while the length of $a3$ is
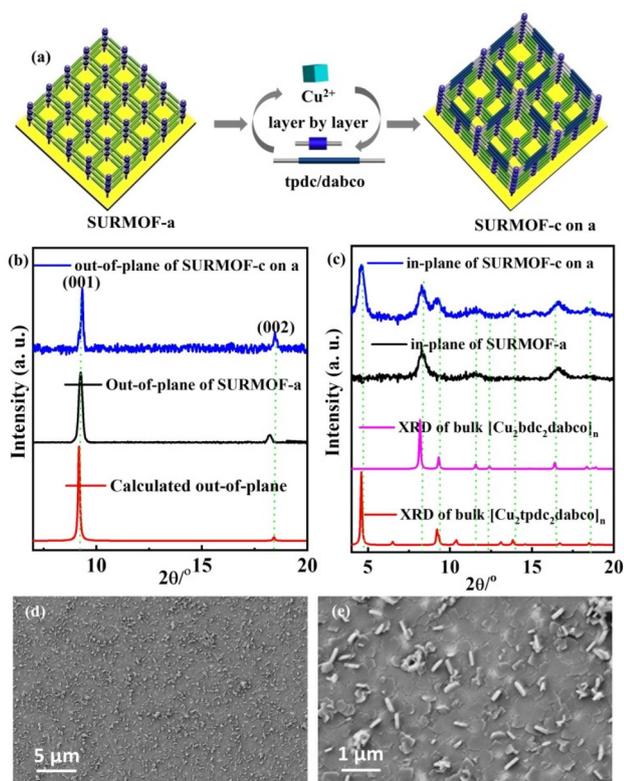
Fig. 2 (a) Preparation process of **SURMOF-c on a**; out-of-plane (b) and in-plane XRD patterns (c) and SEM images (d and e) of **SURMOF-c on a**.
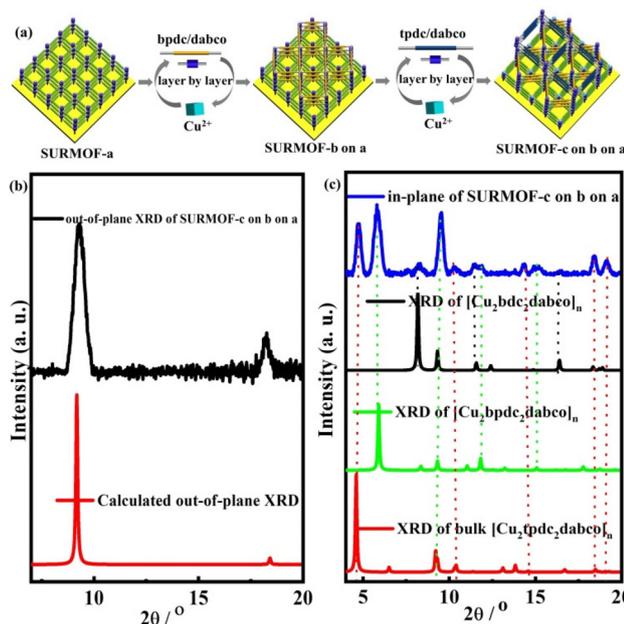

Fig. 3 (a) Preparation process of **SURMOF-c on b on a**; out-of-plane (b) and in-plane XRD patterns (c) of **SURMOF-c on b on a**.

close to that of $\sqrt{2}a2$ (Fig. S15†). Since **SURMOF-a** and **SURMOF-b** have the same c-lattice parameter, the lattice mismatch $[(a2 - a1)/a1]$ is calculated to be 38.6% in a- and

b-lattice parameters. It's noted that the lattice mismatch $[(a3 - a1)/a1]$ between **SURMOF-a** and **SURMOF-c** was calculated to be 77.8%, which was much higher than that of the reported hetero-MOF materials.

The highly oriented, well-defined multiple SURMOFs can offer unique adsorption properties toward guest molecules. In this work, a quartz crystal microbalance (QCM) with a sensing chip is a promising option for this adsorption kinetic study.[49–51] Herein the representative mono-varietal (**SURMOF-a** and **SURMOF-c**) and multiple SURMOFs (**SURMOF-c on a**) were prepared on MUD modified Au QCM electrodes for 30 cycles using the same process. Two kinds of guest molecules ethoxyethane (chain-shape with a size of ~1.0 × 7.0 Å^2) and mesitylene (diameter of ~7.0 Å) with different sizes were selected as the probe molecules since both of them hardly have interactions with SURMOFs and their sizes are largely different. As shown in Fig. 4a, both SURMOFs had high mass uptakes of ethoxyethane, which were calculated to be ~177 μg cm^{-2} for **SURMOF-a** and ~144 μg cm^{-2} for **SURMOF-c**, respectively. To further evaluate the adsorption kinetics, the uptake amount $m(t)$ can be described by an exponential decay equation: $m(t) = m_{eq}(1 - \exp(-t/\tau))$, where τ denotes the time constant, m_{eq} is the equilibrium adsorption and t is the adsorption time. After fitting the uptake curves with the non-linear exponential equation, the time constant (τ) of ethoxyethane adsorption in **SURMOF-a** was 1146 s, which was much slower than the adsorption time (404 s) in **SURMOF-c**. Using the same uptake testing process in the mesitylene adsorption (Fig. 4b) of **SURMOF-a** and **SURMOF-c**, the mass uptake in **SURMOF-a** was calculated to be ~330 μg cm^{-2}, while that in **SURMOF-c** was very low (~26 μg cm^{-2}), which can be attributed to that the pore size (square shape with a size of ~6.7 × 6.7 Å^2 calculated from the space filling model) of **SURMOF-a** is close to the size of mesitylene. In order to study the adsorption kinetic performance of multiple SURMOFs, the representative bi-varietal **SURMOF-c on a** (15 cycles **SURMOF-c** on 15 cycles **SURMOF-a**) was studied. Interestingly, the kinetics adsorption curve of mixed ethoxyethane and mesitylene (1 : 1 v/v%) on **SURMOF-c on a** is not like that of any of the mono-varietal SURMOFs (Fig. 4c); two distinct stages in terms of kinetic adsorption rate can be divided. The first uptake stage is mainly caused by the chain-shaped ethoxyethane with small size, which reached the adsorption capacity of ~86 μg cm^{-2} with fast diffusion (~3 s). In the second stage, the adsorption rate was much slower than that in the first stage, which can be attributed to the main adsorption of large size mesitylene on the **SURMOF-c** layer, causing slow pore diffusion of guest molecules. Finally the total amount of the uptake reached ~245 μg cm^{-2}. To understand the adsorption mechanism, the diffusion models of guest molecules in the SURMOFs are shown in Fig. 4d. Since the pore size of **SURMOF-a** is smaller than that (square shape with a size of ~11.0 × 11.0 Å^2 calculated from the space filling model) of **SURMOF-c**, the small size ethoxyethane has a faster diffusion in **SURMOF-c** than in **SURMOF-c**. The size of mesitylene is close to the pore size of **SURMOF-a** but smaller than that of **SURMOF-c**, resulting in a
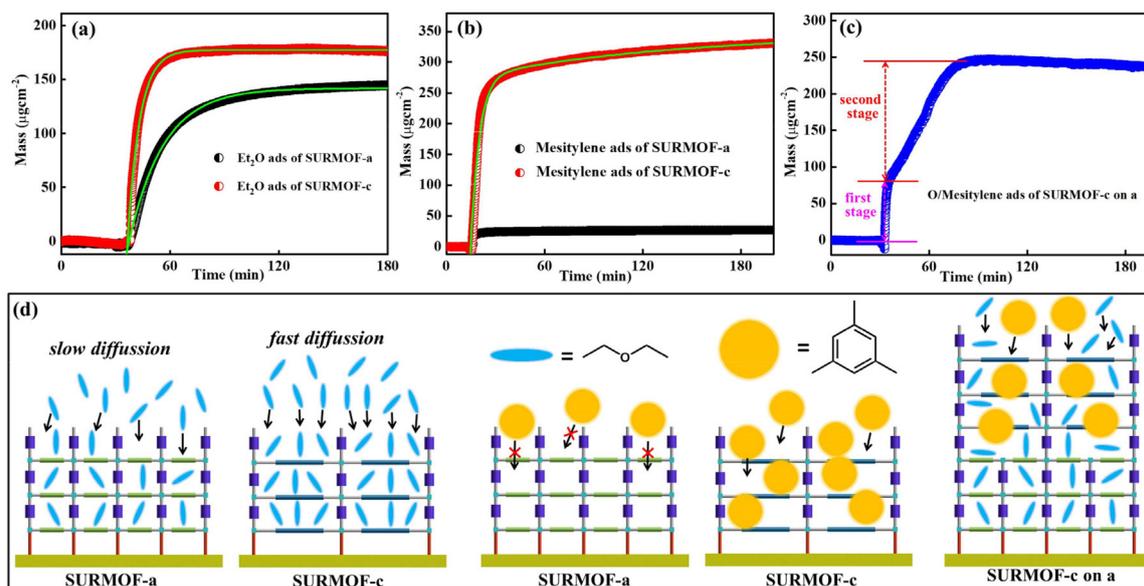
Fig. 4 (a) QCM adsorption curves of Ethoxyethane for **SURMOF-a** and **SURMOF-c**; (b) QCM adsorption curves of mesitylene for **SURMOF-a** and **SURMOF-c**; (c) QCM adsorption curves of mixed ethoxyethane and mesitylene (1 : 1 v/v%) for **SURMOF-c on a**; (d) adsorption model of the related SURMOFs: ethoxyethane adsorption of **SURMOF-a** with slow diffusion and **SURMOF-c** with fast diffusion, mesitylene adsorption of **SURMOF-a** and **SURMOF-c** with different sizes, mixed ethoxyethane and mesitylene (1 : 1 v/v%) adsorption of **SURMOF-c on a**.

huge adsorption difference. Furthermore, the **SURMOF-c on a** with hierarchical pores possessed unique molecule diffusion behavior—first fast diffusion of small molecule ethoxyethane and then slow diffusion of large molecule mesitylene. The advantage of multiple SURMOFs with large lattice mismatch is that the synergistic effect emanated from the different MOF thin films could significantly tune the adsorption kinetic performance.

Conclusions

In summary, we have successfully prepared a series of single and multiple pillar-layered SURMOFs $[Cu_2L_2dabco]_n$ (L = bdc, bpc and tpdc) using a LPE layer by layer pump method. The isostructural SURMOFs with the same c-lattice parameters but different a- and b-lattice parameters result in the successful oriented growth of multiple SURMOFs with high lattice mismatch. Furthermore, the vapor QCM uptakes of ethoxyethane and mesitylene show that the multiple SURMOF has unique adsorption behavior compared to single SURMOFs, demonstrating that such highly lattice mismatched SURMOFs with a synergistic effect have the advantage of tuning the adsorption kinetics performance, which provides new platforms to combine various functional MOFs to extend their applications in thin film based devices and sensors.

Conflicts of interest

There are no conflicts to declare.

Acknowledgements

References

1 L. Jiao, Y. Wang, H. L. Jiang and Q. Xu, Metal-Organic Frameworks as Platforms for Catalytic Applications, *Adv. Mater.*, 2018, **30**, 1703663.

2 K. A. Adegoke, O. R. Adegoke, R. A. Adigun, N. W. Maxakato and O. S. Bello, Two-dimensional metal-organic frameworks: From synthesis to biomedical, environmental, and energy conversion applications, *Coord. Chem. Rev.*, 2022, **473**, 214817.

3 K. Li, Y. Qin, Z. G. Li, T. M. Guo, L. C. An, W. Li, N. Li and X. H. Bu, Elastic properties related energy conversions of coordination polymers and metal-organic frameworks, *Coord. Chem. Rev.*, 2022, **470**, 214692.

4 Q. Ding, Z. Q. Zhang, C. Yu, P. X. Zhang, J. Wang, L. Y. Kong, X. L. Cui, C. H. He, S. G. Deng and H. B. Xing, Separation of propylene and propane with a microporous metal-organic framework via equilibrium-kinetic synergetic effect, *AIChE J.*, 2021, **67**, e17094.

5 R. T. Liu, L. N. Chi, J. M. Feng and X. Z. Wang, MOFs-derived conductive structure for high-performance

1140 | *Inorg. Chem. Front.*, 2023, **10**, 1136–1142

This journal is © the Partner Organisations 2023

removal/release of phosphate as electrode material, *Water Res.*, 2020, **184**, 116198.

6 C. P. Guo, F. H. Duan, S. Zhang, L. H. He, M. H. Wang, J. L. Chen, J. Q. Zhang, Q. J. Jia, Z. H. Zhang and M. Du, Heterostructured hybrids of metal-organic frameworks (MOFs) and covalent-organic frameworks (COFs), *J. Mater. Chem. A*, 2022, **10**, 475–507.

7 L. Y. Xiao, Z. L. Wang and J. Q. Guan, 2D MOFs and their derivatives for electrocatalytic applications: Recent advances and new challenges, *Coord. Chem. Rev.*, 2022, **472**, 214777.

8 Z. X. Li, J. Guo, Y. Wan, Y. T. Qin and M. T. Zhao, Combining metal-organic frameworks (MOFs) and covalent-organic frameworks (COFs): Emerging opportunities for new materials and applications, *Nano Res.*, 2022, **15**, 3514–3532.

9 L. Jiao, J. T. Zhu, Y. Zhang, W. J. Yang, S. Y. Zhou, A. W. Li, C. F. Xie, X. S. Zheng, W. Zhou, S. H. Yu and H. L. Jiang, Non-Bonding Interaction of Neighboring Fe and Ni Single-Atom Pairs on MOF-Derived N-Doped Carbon for Enhanced CO2 Electroreduction, *J. Am. Chem. Soc.*, 2021, **143**, 19417–19424.

10 P. Geng, L. Wang, M. Du, Y. Bai, W. Li, Y. Liu, S. Chen, P. Braunstein, Q. Xu and H. Pang, MIL-96-Al for Li–S Batteries: Shape or Size?, *Adv. Mater.*, 2022, **34**, 2107836.

11 W. Li, X. Guo, P. Geng, M. Du, Q. Jing, X. Chen, G. Zhang, H. Li, Q. Xu, P. Braunstein and H. Pang, Rational Design and General Synthesis of Multimetallic Metal–Organic Framework Nano-Octahedra for Enhanced Li–S Battery, *Adv. Mater.*, 2021, **33**, 2105163.

12 X. Guo, H. Xu, W. Li, Y. Liu, Y. Shi, Q. Li and H. Pang, Embedding Atomically Dispersed Iron Sites in Nitrogen-Doped Carbon Frameworks-Wrapped Silicon Suboxide for Superior Lithium Storage, *Adv. Sci.*, 2022, 2206084.

13 D. Yan, Z. F. Wang and Z. J. Zhang, Stimuli-Responsive Crystalline Smart Materials: From Rational Design and Fabrication to Applications, *Acc. Chem. Res.*, 2022, **55**, 1047–1058.

14 A. M. Rice, W. B. Fellows, E. A. Dolgopolova, A. B. Greytak, A. K. Vannucci, M. D. Smith, S. G. Karakalos, J. A. Krause, S. M. Avdoshenko, A. A. Popov and N. B. Shustova, Hierarchical Corannulene-Based Materials: Energy Transfer and Solid-State Photophysics, *Angew. Chem., Int. Ed.*, 2017, **56**, 4525–4529.

15 V. Stavila, A. A. Talin and M. D. Allendorf, MOF-based electronic and optoelectronic devices, *Chem. Soc. Rev.*, 2014, **43**, 5994–6010.

16 N. J. Hinks, A. C. McKinlay, B. Xiao, P. S. Wheatley and R. E. Morris, Metal organic frameworks as NO delivery materials for biological applications, *Microporous Mesoporous Mater.*, 2010, **129**, 330–334.

17 J. Q. Dong, Y. Liu and Y. Cui, Artificial Metal-Peptide Assemblies: Bioinspired Assembly of Peptides and Metals through Space and across Length Scales, *J. Am. Chem. Soc.*, 2021, **143**, 17316–17336.

18 H. V. Doan, H. A. Hamzah, P. K. Prabhakaran, C. Petrillo and V. P. Ting, Hierarchical Metal-Organic Frameworks with Macroporosity: Synthesis, Achievements, and Challenges, *Nano-Micro Lett.*, 2019, **11**, 281–313.

19 A. Dutta, Y. Pan, J. Q. Liu and A. Kumar, Multicomponent isoreticular metal-organic frameworks: Principles, current status and challenges, *Coord. Chem. Rev.*, 2021, **445**, 214074.

20 X. H. Liu, S. H. Zhang, G. L. Feng, Z. G. Wu, D. Wang, M. D. Albaqami, B. H. Zhong, Y. X. Chen, X. D. Guo, X. T. Xu and Y. Yamauchi, Core-Shell MOF@COF Motif Hybridization: Selectively Functionalized Precursors for Titanium Dioxide Nanoparticle-Embedded Nitrogen-Rich Carbon Architectures with Superior Capacitive Deionization Performance, *Chem. Mater.*, 2021, **33**, 1657–1666.

21 C. Liu, J. Wang, J. J. Wan and C. Z. Yu, MOF-on-MOF hybrids: Synthesis and applications, *Coord. Chem. Rev.*, 2021, **432**, 213743.

22 V. Chernikova, O. Shekhah, I. Spanopoulos, N. T. B. Pantelis and M. Eddaoudi, Liquid phase epitaxial growth of heterostructured hierarchical MOF thin films, *Chem. Commun.*, 2017, **53**, 6191–6194.

23 K. Ikigaki, K. Okada, Y. Tokudome, T. Toyao, P. Falcaro, C. J. Doonan and M. Takahashi, MOF-on-MOF: Oriented Growth of Multiple Layered Thin Films of Metal-Organic Frameworks, *Angew. Chem., Int. Ed.*, 2019, **58**, 6886–6890.

24 R. Haldar and C. Woll, Hierarchical assemblies of molecular frameworks-MOF-on-MOF epitaxial heterostructures, *Nano Res.*, 2021, **14**, 355–368.

25 R. Haldar, L. Heinke and C. Woll, Advanced Photoresponsive Materials Using the Metal-Organic Framework Approach, *Adv. Mater.*, 2019, **32**, 1905227.

26 L. Sun, M. G. Campbell and M. Dinca, Electrically Conductive Porous Metal-Organic Frameworks, *Angew. Chem., Int. Ed.*, 2016, **55**, 3566–3579.

27 I. S. Kim, S. Ahn, N. A. Vermeulen, T. E. Webber, L. C. Gallington, K. W. Chapman, R. L. Penn, J. T. Hupp, O. K. Farha, J. M. Notestein and A. B. F. Martinson, The Synthesis Science of Targeted Vapor-Phase Metal-Organic Framework Postmodification, *J. Am. Chem. Soc.*, 2020, **142**, 242–250.

28 J. R. Luo, Y. Li, H. C. Zhang, A. L. Wang, W. S. Lo, Q. Dong, N. Wong, C. Povinelli, Y. C. Shao, S. Chereddy, S. Wunder, U. Mohanty, C. K. Tsung and D. W. Wang, A Metal-Organic Framework Thin Film for Selective Mg2+ Transport, *Angew. Chem., Int. Ed.*, 2019, **58**, 15313–15317.

29 B. Ghalei, K. Wakimoto, C. Y. Wu, A. P. Isfahani, T. Yamamoto, K. Sakurai, M. Higuchi, B. K. Chang, S. Kitagawa and E. Sivaniah, Rational Tuning of Zirconium Metal-Organic Framework Membranes for Hydrogen Purification, *Angew. Chem., Int. Ed.*, 2019, **58**, 19034–19040.

30 I. Stassen, M. Styles, G. Grenci, H. Van Gorp, W. Vanderlinden, S. De Feyter, P. Falcaro, D. De Vos, P. Vereecken and R. Ameloot, Chemical vapour deposition of zeolitic imidazolate framework thin films, *Nat. Mater.*, 2016, **15**, 304–310.

31 E. Virmani, J. M. Rotter, A. Mahringer, T. von Zons, A. Godt, T. Bein, S. Wuttke and D. D. Medina, On-Surface

This journal is © the Partner Organisations 2023

Inorg. Chem. Front., 2023, **10**, 1136–1142 | **1141**

Synthesis of Highly Oriented Thin Metal-Organic Framework Films through Vapor-Assisted Conversion, *J. Am. Chem. Soc.*, 2018, **140**, 4812–4819.

32 G. Delen, M. Monai, F. Meirer and B. M. Weckhuysen, In situ Nanoscale Infrared Spectroscopy of Water Adsorption on Nanoislands of Surface-Anchored Metal-Organic Frameworks, *Angew. Chem., Int. Ed.*, 2021, **60**, 1620–1624.

33 J. L. Zhuang, M. Kind, C. M. Grytz, F. Farr, M. Diefenbach, S. Tussupbayev, M. C. Holthausen and A. Terfort, Insight into the Oriented Growth of Surface-Attached Metal-Organic Frameworks: Surface Functionality, Deposition Temperature, and First Layer Order, *J. Am. Chem. Soc.*, 2015, **137**, 8237–8243.

34 R. Haldar, S. Diring, P. K. Samanta, M. Muth, W. Clancy, A. Mazel, S. Schlabach, F. Kirschhofer, G. Brenner-Weiss, S. K. Pati, F. Odobel and C. Woll, Enhancing Selectivity and Kinetics in Oxidative Photocyclization by Supramolecular Control, *Angew. Chem., Int. Ed.*, 2018, **57**, 13662–13665.

35 Y. H. Xiao, P. Weidler, S. S. Lin, C. Woll, Z. G. Gu and J. Zhang, Chiral Metal-Organic Cluster Induced High Circularly Polarized Luminescence of Metal-Organic Framework Thin Film, *Adv. Funct. Mater.*, 2022, **32**, 2204289.

36 Z. G. Gu and J. Zhang, Epitaxial growth and applications of oriented metal-organic framework thin films, *Coord. Chem. Rev.*, 2019, **378**, 513–532.

37 Z. B. Wang, J. X. Liu, B. Lukose, Z. G. Gu, P. G. Weidler, H. Gliemann, T. Heine and C. Woll, Nanoporous Designer Solids with Huge Lattice Constant Gradients: Multiheteroepitaxy of Metal-Organic Frameworks, *Nano Lett.*, 2014, **14**, 1526–1529.

38 D. Zacher, A. Baunemann, S. Hermes and R. A. Fischer, Deposition of microcrystalline [Cu-3(btc)(2)] and [Zn-2(bdc)(2)(dabco)] at alumina and silica surfaces modified with patterned self assembled organic monolayers: evidence of surface selective and oriented growth, *J. Mater. Chem.*, 2007, **17**, 2785–2792.

39 Y. Wu, S. Henke, G. Kieslich, I. Schwedler, M. S. Yang, D. A. X. Fraser and D. O'Hare, Time-Resolved InSitu X-ray Diffraction Reveals Metal-Dependent Metal-Organic Framework Formation, *Angew. Chem., Int. Ed.*, 2016, **55**, 14081–14084.

40 C. J. Lu, T. Ben, S. X. Xu and S. L. Qiu, Electrochemical Synthesis of a Microporous Conductive Polymer Based on a Metal-Organic Framework Thin Film, *Angew. Chem., Int. Ed.*, 2014, **53**, 6454–6458.

41 S. M. Chen, M. Liu, Z. G. Gu, W. Q. Fu and J. Zhang, Chiral Chemistry of Homochiral Porous Thin Film with Different Growth Orientations, *ACS Appl. Mater. Interfaces*, 2016, **8**, 27332–27338.

42 Z. G. Gu, Z. Chen, W. Q. Fu, F. Wang and J. Zhang, Liquid-Phase Epitaxy Effective Encapsulation of Lanthanide Coordination Compounds into MOF Film with Homogeneous and Tunable White-Light Emission, *ACS Appl. Mater. Interfaces*, 2015, **7**, 28585–28590.

43 O. Shekhah, H. Wang, D. Zacher, R. A. Fischer and C. Woll, Growth Mechanism of Metal-Organic Frameworks: Insights into the Nucleation by Employing a Step-by-Step Route, *Angew. Chem., Int. Ed.*, 2009, **48**, 5038–5041.

44 D. Zacher, O. Shekhah, C. Woll and R. A. Fischer, Thin films of metal-organic frameworks, *Chem. Soc. Rev.*, 2009, **38**, 1418–1429.

45 B. Liu, O. Shekhah, H. K. Arslan, J. X. Liu, C. Woll and R. A. Fischer, Enantiopure Metal-Organic Framework Thin Films: Oriented SURMOF Growth and Enantioselective Adsorption, *Angew. Chem., Int. Ed.*, 2012, **51**, 807–810.

46 O. Shekhah, K. Hirai, H. Wang, H. Uehara, M. Kondo, S. Diring, D. Zacher, R. A. Fischer, O. Sakata, S. Kitagawa, S. Furukawa and C. Woll, MOF-on-MOF heteroepitaxy: perfectly oriented [Zn-2(ndc)(2)(dabco)](n) grown on [Cu-2(ndc)(2)(dabco)](n) thin films, *Dalton Trans.*, 2011, **40**, 4954–4958.

47 O. Shekhah, H. Wang, M. Paradinas, C. Ocal, B. Schupbach, A. Terfort, D. Zacher, R. A. Fischer and C. Woll, Controlling interpenetration in metal-organic frameworks by liquid-phase epitaxy, *Nat. Mater.*, 2009, **8**, 481–484.

48 Z. G. Gu, S. Grosjean, S. Brase, C. Woll and L. Heinke, Enantioselective adsorption in homochiral metal-organic frameworks: the pore size influence, *Chem. Commun.*, 2015, **51**, 8998–9001.

49 D. X. Xue, Y. Belmabkhout, O. Shekhah, H. Jiang, K. Adil, A. J. Cairns and M. Eddaoudi, Tunable Rare Earth fcu-MOF Platform: Access to Adsorption Kinetics Driven Gas/Vapor Separations via Pore Size Contraction, *J. Am. Chem. Soc.*, 2015, **137**, 5034–5040.

50 V. Stavila, C. Schneider, C. Mowry, T. R. Zeitler, J. A. Greathouse, A. L. Robinson, J. M. Denning, J. Volponi, K. Leong, W. Quan, M. Tu, R. A. Fischer and M. D. Allendorf, Thin Film Growth of nbo MOFs and their Integration with Electroacoustic Devices, *Adv. Funct. Mater.*, 2016, **26**, 1699–1707.

51 M. Tu, S. Wannapaiboon, K. Khaletskaya and R. A. Fischer, Engineering Zeolitic-Imidazolate Framework (ZIF) Thin Film Devices for Selective Detection of Volatile Organic Compounds, *Adv. Funct. Mater.*, 2015, **25**, 4470–4479.

1142 | *Inorg. Chem. Front.*, 2023, **10**, 1136–1142

This journal is © the Partner Organisations 2023